Eur. Phys. J. B **18**, 163–181 (2000)

THE EUROPEAN PHYSICAL JOURNAL B

EDP Sciences

Critical ruptures

A. Johansen[1] and D. Sornette[1,2,3,a]

[1] Institute of Geophysics and Planetary Physics, University of California, Los Angeles, California 90095, USA
[2] Department of Earth and Space Science, University of California, Los Angeles, California 90095, USA
[3] Laboratoire de Physique de la Matière Condensée[b], and Université de Nice-Sophia Antipolis, BP 71, Parc Valrose, 06108 Nice Cedex 2, France

Received 6 July 2000

Abstract. The fracture of materials is a catastrophic phenomenon of considerable technological and scientific importance. Here, we analysed experiments designed for industrial applications in order to test the concept that, in heterogeneous materials such as fiber composites, rocks, concrete under compression and materials with large distributed residual stresses, rupture is a genuine critical point, *i.e.*, the culmination of a self-organization of damage and cracking characterized by power law signatures. Specifically, we analyse the acoustic emissions recorded during the pressurisation of spherical tanks of kevlar or carbon fibers pre-impregnated in a resin matrix wrapped up around a thin metallic liner (steel or titanium) fabricated and instrumented by Aérospatiale-Matra Inc. These experiments are performed as part of a routine industrial procedure which tests the quality of the tanks prior to shipment. We find that the seven acoustic emission recordings of seven pressure tanks which was brought to rupture exhibit clear acceleration in agreement with a power law "divergence" expected from the critical point theory. In addition, we find strong evidence of log-periodic corrections that quantify the intermittent succession of accelerating bursts and quiescent phases of the acoustic emissions on the approach to rupture. An improved model accounting for the cross-over from the non-critical to the critical region close to the rupture point exhibits interesting predictive potential.

PACS. 81.40.Np Fatigue, corrosion fatigue, embrittlement, cracking, fracture and failure – 05.70.Jk Critical point phenomena

1 Plan of the study

In this paper, we first present in Section 2 a brief review of the "critical rupture" concept with an emphasis on the role of heterogeneity. Section 3 describes the experimental systems and the properties of the acoustic emission time series that we analyse with three theoretical formulas derived from the critical rupture concept. We present a brief justification for these three power laws. Section 4 gives the results obtained on the acoustic emission energy release rate on seven systems. Section 5 analyses the cumulative energy releases of these seven systems. Section 6 describes the relative merits of the three power law formulas for the prediction of the critical pressure of rupture and Section 7 concludes.

2 Review of the "critical rupture" concept

2.1 Background

The damage and fracture of materials is of enormous technological interest due to their economic and human cost. They cover a wide range of phenomena like, *e.g.*, cracking of glass, aging of concrete, the failure of fiber networks in the formation of paper and the breaking of a metal bar subject to an external load. Failure of composite systems are of utmost importance in naval, aeronautics and space industry [1]. By the term composite, we refer to materials with heterogeneous microscopic structures and also to assemblages of macroscopic elements forming a superstructure. Chemical and nuclear plants suffer from cracking due to corrosion either of chemical or radioactive origin, aided by thermal and/or mechanical stress.

Despite the large amount of experimental data and the considerable effort that has been undertaken by material scientists [2], many questions about fracture have not been answered yet. There is no comprehensive understanding of rupture phenomena but only a partial classification in restricted and relatively simple situations. This lack of fundamental understanding is indeed reflected in the absence of reliable prediction methods for rupture based on a suitable monitoring of the stressed system. Not only is there a lack of theoretical understanding of the reliability of a system, but the empirical laws themselves have often limited value. What we need are models that incorporate the underlying physics to identify and use relevant precursory patterns. Here, we propose innovative steps

[a] e-mail: sornette@moho.ess.ucla.edu
[b] CNRS UMR6622

in this direction that are based on two key concepts : the role of heterogeneity and the possible existence of a hierarchy of characteristic scales.

Many material ruptures occur by a "one crack" mechanism and a lot of effort is being devoted to the understanding, detection and prevention of the nucleation of cracks [3,4]. Exceptions to the "one crack" rupture mechanism are heterogeneous materials such as fiber composites, rocks, concrete under compression and materials with large distributed residual stresses. The common property shared by these systems is the existence of large inhomogeneities, that often limit the use of effective medium theories for the elastic and more generally the mechanical properties. In these systems, failure may occur as the culmination of a progressive damage involving complex interactions between multiple defects and the growing of micro-cracks. In addition, other relaxation, creep, ductile, or plastic behaviors, possibly coupled with corrosion effects, may come into play. Many important practical applications involve the coupling between mechanic and chemical effects with the competition between several characteristic time scales. Application of stress may act as a catalyst of chemical reactions [5] or, reciprocally, chemical reactions may lead to bond weakening [6] and thus promote failure. A dramatic example is the aging of present aircrafts due to repeating loading in a corrosive environment [7]. The interaction between multiple defects and the existence of several characteristic scales present a considerable challenge to the modeling and prediction of rupture. Those are the systems and problems that will guide our modeling efforts.

2.2 Previous statistical physics models

2.2.1 Scaling and critical point

The analogy between rupture and criticality has been already proposed in [8], which analyzed the Young modulus and stress/strain relationships of various materials as a function of temperature and damage. This work brought up the analogy between the fracture/compaction behavior and that of the liquid/gas phase transition *a la* van der Waals.

Motivated by the multi-scale nature of ruptures in heterogeneous systems and by analogies with the percolation model [9], de Arcangelis *et al.* first suggested [10] in the mid-eighties that rupture of sufficiently heterogeneous media would exhibit some universal properties, in a way possibly similar to critical phase transitions. The idea was to build on the knowledge accumulated in statistical physics on the so-called $N-$body problem and cooperative effects in order to describe multiple interactions between defects. However, most of the models were extremely naive and essentially all of them quasi-static with rather unrealistic loading rules [10–14]. Some suggestive scaling laws were found to describe size effects and damage properties [14,15], but the relevance to real materials was not convincingly demonstrated with a few exceptions: for instance, percolation theory has been proposed as a theoretical explanation for the experimentally based Coffin-Manson law of low cycle fatigue [16]. The interest of physicists for the modeling of rupture in heterogeneous media seems to have decreased since then except for a few active groups.

In 1992, the first model of rupture with a realistic dynamical law for the evolution of damage was introduced. It was initially formulated in the framework of electric breakdown under the name of the "thermal fuse model" [18] : when subjected to a given current, a fuse heats up due to a generalized Joule effect and eventually breaks down when its temperature reaches the melting threshold. Later, it was reformulated in [19] by showing that it is exactly equivalent to a (scalar) anti-plane mechanical model of rupture with elastic interaction in which the temperature becomes a local damage variable. This model accounts for space-dependent elastic and rupture properties, has a realistic loading and produces many growing interacting micro-cracks with an organization which is a function of the damage-stress law. It was found that, under a step-function stress loading, the total rate of damage, as measured for instance by the elastic energy released per unit time, on average increases as a power law of the time-to-failure. In this model, rupture was indeed found to occur as the culmination of the progressive nucleation, growth and fusion between micro-cracks, leading to a fractal network, but the exponents were found to be non-universal and a function of the damage law. This model has since then been found to describe correctly the experiments on the electric breakdown of insulator-conducting composites [20]. Another application of the thermal fuse model is damage by electro-migration of polycrystalline metal films [21]. See also [19] for relations with dendrites and fronts propagation.

In 1991–1995, it was proposed and tested on a real engineering composite structure the concept that failure in fiber composites may be described similarly, namely that the rate of damage would exhibit a "critical" behavior [22]. This critical behavior corresponds to an acceleration of the rate of energy release or to a deceleration, depending on the nature and range of the stress transfer mechanism and on the loading procedure. Based on general consideration on the nature of the experimental signatures of critical rupture, it was proposed that the power law behavior of the time-to-failure analysis should be corrected for the presence of log-periodic modulations [22] as signatures of a hierarchy of characteristic scales in the rupture process. This method is now been used by the French Aerospace company Aérospatiale-Matra on pressure tanks made of kevlar-matrix and carbon-matrix composites embarked on the European Ariane 4 and 5 rockets. In a nutshell, the method consists in this application in recording acoustic emissions under constant stress rate and the acoustic emission energy as a function of stress is fitted by the above log-periodic critical theory [22]. One of the parameter is the time of failure and the fit thus provides a "prediction" when the sample is not brought to failure

in the first test [23]. Good predictive performances have been reported (Anifrani, private communication). Since we now have a better understanding of the mechanisms at the origin of the hierarchical self-organization in rupture [24–26] which seems to apply to some other systems as well [27,28], here we re-examine the critical rupture concept and the evidence for the existence of log-periodic corrections to scaling [22,37]. This study is based on the analysis of 7 acoustic emission recordings of 7 pressure tank structures brought to rupture. The experiments were performed at Aérospatiale-Matra Inc. according to the procedure described in [22]. The acoustic emissions recorded during the loading phase up to rupture were made available to us. We also present preliminary tests of the predictive skills, in particular using an extension of the theory which allows us to incorporate the cross-over regime from the non-critical to the critical regime [35].

2.2.2 The role of heterogeneities

A key parameter is the degree and nature of disorder. This was considered early by Mogi [29], who showed experimentally on a variety of materials that, the larger the disorder, the stronger and more useful are the precursors to rupture. For a long time, the Japanese research effort for earthquake prediction and risk assessment was based on this very idea [30].

The role of heterogeneities on the nature of rupture has been quantified using a spring-block model with stress transfer over limited range and on the democratic fiber bundle model [31]. The former model does not claim realism but attempts rather to capture the role of limited stress transfer and heterogeneity. The heterogeneity was found to play the role of a relevant field: systems with limited stress amplification exhibit a tri-critical transition [32], from a Griffith-type abrupt rupture (first-order) regime to a progressive damage (critical) regime as the disorder increases. This effect has also been demonstrated on a simple mean-field model of rupture, known as the democratic fiber bundle model [33]. In a two-dimensional spring-block model of surface fracture, the stress can be released by breaking of springs *and* block slips [31]. This spring-block model may represent schematically the experimental situation where a balloon covered with paint or dry resin is progressively inflated. An industrial application may be for instance a metallic tank with carbon or kevlar fibers impregnated in a resin matrix wrapped up around it which is slowly pressurized [22], as we report in this paper. As a consequence, it elastically deforms, transferring tensile stress to the overlayer. Slipping (called fiber-matrix delamination) and cracking can thus occur in the overlayer. In [31], this process is modeled by an array of blocks which represents the overlayer on a coarse grained scale in contact with a surface with solid friction contact. The solid friction will limit stress amplification. The stress-strain curves for different values of the disorder Δ, here quantified by the width of the distribution of initial positions of the blocks which captures the effect of residual stresses in the material (but does not explore the other dimensions of disorder), show a larger softening and rounding as disorder increases. The phase diagram of the fracturing in the $(\Delta; F_c/F_s)$ plane, where F_c (resp. F_s) is the rupture (resp. sliding) threshold shows that, for fixed $F_c/F_s < 2.9$, increasing the disorder Δ allows the system to go from a first-order behaviour to a critical regime. The fact that the disorder is so relevant as to create the analog of a tri-critical behavior can be traced back to the existence of solid friction on the blocks which ensures that the elastic forces in the springs are carried over a bounded distance (equal to the size of a slipping "avalanche") during the stress transfer induced by block motions. In this context, we note that the importance of heterogeneity in the context of fiber composites has also been stressed in [34].

In the presence of long-range elasticity, disorder is found to be always relevant leading to a critical rupture. However, the disorder controls the width of the critical region [35]. The smaller it is, the smaller will be the critical region, which may become too small to play any role in practice. This has been confirmed by simulations of the thermal fuse model mentioned above [18]. The damage rate on approach to failure for different disorder can be rescaled onto a universal master curve [35].

Numerical simulations of Sahimi and Arbati [36] have confirmed that, near the global failure point, the cumulative elastic energy released during fracturing of heterogeneous solids with long-range elastic interactions follows a power law with log-periodic corrections to the leading term consistent with previous results [22-28]. The presence of log-periodic correction to scaling in the elastic energy released has also been demonstrated numerically for the thermal fuse model [37,26] using a novel averaging procedure, called the "canonical ensemble averaging". A recent experimental study of rupture of fiber-glass composites has also confirmed the critical scenario [38].

These results indicate that the "critical" behavior is not restricted to limited stress amplification but may well pertain to a much broader class of systems. This needs to be investigated more. In quasi-static models of rupture [14,15], numerical simulations and perturbation expansions have shown the existence of three main regimes, depending on the distribution $p(x)$ of rupture thresholds x. If $p(x) \sim x^{\phi_0 - 1}$ for $x \to 0$ and $p(x) \sim x^{-(1+\phi_\infty)}$ for $x \to +\infty$, then the three regimes depend on the relative value of ϕ_0 and ϕ_∞ compared to two critical values ϕ_0^c and ϕ_∞^c. The "weak disorder" regime occurs for $\phi_0 > \phi_0^c$ (few weak elements) and $\phi_\infty > \phi_\infty^c$ (few strong elements) and boils down essentially to the nucleation of a "one-crack" run-away. For $\phi_0 \leq \phi_0^c$ (many weak elements) and $\phi_\infty > \phi_\infty^c$ (few strong elements), the rupture is controlled by the weak elements, with important size effects. The damage is diffuse but presents a structuration at large scales. For $\phi_0 > \phi_0^c$ (few weak elements) and $\phi_\infty \leq \phi_\infty^c$ (many strong elements), the rupture is controlled by the strong elements : the final damage is diffuse and the density of broken elements goes to a non-vanishing constant. This third case is very similar to the percolation

models of rupture and it has been shown that percolation is retrieved in the limit of very large disorder [13].

2.2.3 Qualitative physical scenario

A qualitative physical picture for the progressive damage of an heterogeneous system leading to global failure emerges from all these results. First, single isolated defects and micro-cracks nucleate which then, with the increase of load or time of loading, both grow and multiply leading to an increase of the density of defects per unit volume. As a consequence, defects begin to merge until a "critical density" is reached. Uncorrelated percolation [9] provides a starting modeling point valid in the limit of very large disorder [13,39]. For realistic systems, long-range correlations transported by the stress field around defects and cracks make the problem much more subtle. Time dependence is expected to be a crucial aspect in the process of correlation building in these processes. As the damage increases, a new "phase" appears, where micro-cracks begin to merge leading to screening and other cooperative effects. Finally, the main fracture is formed causing global failure. The nature of this global failure may be abrupt ("first-order") or "critical" depending of the type of heterogeneities influencing load transfer and stress relaxation mechanisms. In the "critical" case, the failure of composite systems may often be viewed, in simple intuitive terms, as the result of a correlated percolation process. However, the challenge is to describe the transition from damage and corrosion processes at a microscopic level to macroscopic failure.

3 Data and methodology

3.1 The experimental systems

The systems used in our study are spherical tanks of radius of 0.2 to 0.42 m, made of kevlar or carbon fibers pre-impregnated in a resin matrix wrapped up around a thin metallic liner (steel or titanium). They are fabricated and instrumented by Aérospatiale-Matra Inc. In a typical experiment, each tank is pressurized by increasing the internal water content at a constant pressure rate of 3 to 6 bars per second. Acoustic emission signals are recorded from three to six acoustic transducers with resonant frequency of 150 kHz, placed at equal distances on the equator. Acoustic emissions characterize rather faithfully the irreversible motions and damages occurring within the composites under increasing load. The acoustic emissions were recorded by a Locan-At from Euro Physical Acoustics Inc, with tunings (thresholds, gains, Peak Definition Time, Hit Definition Time, Hit Lock-out Time) adjusted for each experiment. The output of the Locan-At is a list of acoustic events with their time, the pressure at which they occurred, their duration, their amplitude and a measure of their energy. In the sequel, we analyse the files giving the energy of all recorded acoustic emission events as a function of pressure.

Acoustic emissions are mechanical waves produced by sudden movements in stressed materials. They occur in a wide range of materials, structures and processes, from the largest scale (earthquakes) to the smallest one (dislocation motions). Acoustic emission has been found to be a delicate technique to use since each loading is unique and tests the whole structure. Contamination by noise is a real problem. Notwithstanding the development of numerous acoustic emission structural testing procedures [40,41], their practical implementations for prediction purpose have not been found reliable. The acoustic emission technique differs from most other non-destructive methods in that acoustic emissions originate from within the material and results from high-frequency motions, while most methods detect existing geometrical heterogeneities. A large body of research in the mechanical literature has thus focused on the identification of the types of motions that generate acoustic emissions and how their signatures can be associated with their sources. Such sudden material motions can be due to crack nucleation and growth, fiber-matrix delamination, fiber rupture, etc. In the present work, we focus rather on the global view that emerges by analyzing the acoustic emission times series over the whole lifetime of the pressure ramp up to rupture.

We analyse 7 acoustic emission data sets recorded during the pressure ramp up to rupture of 7 distinct composite pressure tanks listed below in Table 1 with some of the characteristics of the experiments. The analysis was not performed on the raw data sets due to a number of experimental factors such as unreliable measurements, limited resolution as well as physical considerations. First, the data was truncated in the upper and lower ends. The reason for the latter is that the recordings made for very low pressures are irrelevant to the rupture process and are unreliable since the low level of acoustic emissions can easily be confused with exterior noise. This truncation was made at 100 bars so that all recordings start at pressure larger or equal to this value. Some data sets did not have recordings for such low pressures and was hence not truncated. The upper endpoint was identified as the first point where the maximum pressure was recorded. The data files were changed into files of binned data using a binning equal to the resolution of the pressure measurement, specifically 1 bar. The maximum value of the acoustic emission for each data set has been normalized to 1 000 in order to make the numerical treatment similar for all 7 experiments.

3.2 Theory

We have used three increasingly sophisticated mathematical formulas to model the acoustic emission time series. The first one reads

$$f(p) = A + B(p_c - p)^z \tag{1}$$

and has *a priori* 3 adjustable parameters, since p_c is imposed as the time of rupture. Here, f is the acoustic emission energy recorded upon loading, *i.e.* increasing the pressure p up to rupture which, theoretically, should occur

at p_c. The important parameters are the critical value p_c of the pressure at rupture and the exponent z (in general negative), which quantifies the acceleration of the acoustic emission rate. This is the fundamental representation of rupture seen as a critical point in the time-to-failure analysis.

The second formula

$$f(p) = A + B(p_c - p)^z + C(p_c - p)^z \cos(\omega \ln(p_c - p) - \phi) \quad (2)$$

contains an additional term with relative weight C/B, describing a so-called log-periodic correction to scaling [22,26]. Basically, this formula means that the power law acceleration is modulated by downs and ups organized as a geometrical series converging to p_c. In other words, the intermittent accelerations and quiescences of the acoustic emissions around the average power law acceleration are more and more closely spaced as rupture is approached. Mathematically, this log-periodic structures can be represented as the real part of a correction to scaling of the form $C(p_c - p)^{z+i\omega}$, *i.e.*, by a complex exponent. The imaginary part ω has the meaning of a logarithmic angular frequency and defines the scaling factor $\lambda = \exp[\pi/\omega]$ of the geometrical series of alternating peaks and troughs. The phase ϕ is of no consequence as it accommodates the specific choice of the pressure unit: $\omega \ln(p_c - p) - \phi = \omega \ln[(p_c - p)/p_0]$ by the definition $\phi = -\omega \ln p_0$. From a general view point, log-periodic oscillations are the hallmark of a discrete hierarchical structure obeying a discrete scale invariance symmetry [26]. Expression (2) has been proposed previously on the basis of a discrete renormalization group approach to rupture [22,26]. Detailed theoretical and numerical analysis of ensemble of interacting cracks have shown that such discrete hierarchy can self-organize from a cascade of Mullins-Sekerka instabilities [25].

The third formula

$$f(p) = A + B(\tanh((p_c - p)/\tau))^z + C(\tanh((p_c - p)/\tau))^z \times \cos(\omega \ln(\tanh((p_c - p)/\tau)) - \phi) \quad (3)$$

adds a new ingredient and is obtained from (2) by replacing $p_c - p$ by $\tanh((p_c - p)/\tau)$. It is based on a parametric representation of the numerical study of Sornette and Andersen [35], who found clear evidence of scaling of the macroscopic elastic modulus and of the elastic energy release rate as a function of time-to-rupture in the thermal fuse model [18] beyond the pure critical power law regime: this allowed them to collapse neatly the numerical simulations over more than five decades in time and more than one decade in disorder amplitude onto a single master curve that has the following properties. It is a pure power law like (1) close to rupture (critical region); far from rupture where only few damage events occur (non-critical region), it relaxes exponentially to a constant value. The simplest functional form that captures these two regimes and interpolates smoothly between them is $[\tanh((p_c - p)/\tau)]^z$, which reduces to (1) for $p_c - p \ll \tau$ and goes exponentially to the constant 1 for $p_c - p \gg \tau$. The characteristic pressure τ sets the crossover scale between the critical and non-critical regime. The analysis [35] was based on averages of several tens of independent samples. As shown in [37], ensemble averaging destroys log-periodic oscillations due to the random phase ϕ which can vary from sample to sample. When studying specific realisations as performed below, these log-periodic structures have to be considered as potentially important. This is why we enrich the hyperbolic tangent formula with the log-periodic corrections associated with equation (2), so that expression (3) reduces to (2) for $p_c - p \ll \tau$, with new definitions of B and C swallowing the dependence in τ.

For each acoustic emission time series, we have analysed both the energy rate as well as its cumulative. The rational for studying the cumulative acoustic emission as a function of applied pressure is that taking the cumulative is a low-pass filter that smoothen very significantly the noise and usually provides better signals with higher signal-over-noise ratio. For our purpose however, it has been shown to reduce significantly genuine log-periodic oscillations present in the original data [42]. We thus find useful to perform the analysis of both the binned (energy rate) and its cumulative, which present complementary values. Since the cumulative data is a low-pass filtered version of the binned data, we first use equation (1) to fit it. The cumulative data will also be presented in a non-parametric fashion in double logarithmic plots to show direct visual confirming evidence of the power law regime (1) close to rupture. The two other formulas (2) and (3) are applied to the cumulative data where a better performance by equation (3) would indicate the presence of a transition from exponential to a power law increase in the energy release rate as discussed above.

4 Analysis of the energy release rate

For the analysis of the energy release rate, a second truncation was made for both the lower and upper ends of the pressure interval. The lower endpoint was defined as the point where the acceleration in the cumulative energy release takes place. The size of this truncation varies considerably from data set to data set. For the files containing data all the way up to p_c (data sets 1, 2, 3, 4, 6), the upper endpoint was simply chosen as the point where the energy release rate had its maximum, thus removing only a few points. For the two data sets (5,7), where the last point is far from p_c, no truncation was performed.

The results were encouraging for all data sets. In Table 1, we see the values of the physical parameters for the best fit of each data set with equation (2). Use of equation (1) for the energy release rate is unreliable due to the huge fluctuations shown in Figure 1. The fits were performed using the "amoeba-search" algorithm [43] minimizing the variance of the fit to the data. We stress that all three linear variables A, B and C are slaved to the other nonlinear variables by imposing the condition that, at a local minimum, the variance has zero first derivative with respect to these variables. Hence, they should

Table 1. Parameter values for fits with equation (2) to the energy release rate. The fits are shown in Figure 1. All pressure tanks are made of Kevlar composite except tank 2 which is a carbon composite.

Set #	# points	# fits	$p_{\min}$	fit p_c	true p_c	p_{last}	z	ω
1	≈ 170	1	110.5	707	713	703	-1.4	5.4
2	≈ 170	3	102.5	674	673	669	-2.1	10.5
3	≈ 70	1	538.5	772	764	764	-0.7	4.5
4	≈ 70	1	334.5	758	756	753	-2.0	4.9
5	≈ 170	2	110.5	717, 738	797	713	$-1.4, -1.0$	10.1, 11.5
6	≈ 180	1	136.5	738	734	734	-1.1	4.7
7	≈ 120	1	283.5	672	797	661	-1.5	10.5

not be regarded as free parameters, but are calculated solving three linear equations using standard techniques including pivoting. Note, in addition, that the phase ϕ in (2) is just a (pressure) unit and the coefficients A, B and C have all dimensions of energy. The key physical variables are thus p_c, z and ω.

The corresponding plots are shown in Figure 1. The best fit is defined as the fit with the lowest r.m.s. (root-mean-square) as well as reasonable values for ω. Specifically, this means that we do not consider solutions with $\omega \lesssim 1$ and $\omega \gtrsim 14$. The reason is that too large values for ω indicates noise-fitting. This means that for data set 5 and 7, the minimum with the lowest r.m.s. was discarded because $\omega = 25$ and $\omega = 17$, respectively. For data set 5, we list the two best minima. Too small values for ω mean that the fit is not truly log-periodic with less than one oscillation. The corresponding log-periodic correction to the pure power law is thus not valid.

Table 1 shows that the log-angular frequencies ω cluster around two values $\omega \approx 5$ or $\omega \approx 10$, corresponding to a frequency multiplexing (doubling), as observed also in diffusion-limited-aggregation (frequency doubling) [28] and in 2D-freely decaying turbulence (frequency tripling) [44]. Another noticeable feature is that the exponent is rather well defined at $z \approx -1.4 \pm 0.7$, notwithstanding the well-known difficulties in estimating critical exponents, especially in such noisy data as analysed here. The values obtained for the critical pressure p_c are all rather close to the last point in the data sets with the exception of the second minimum for data set 5. This means that equation (2) does a good job of parameterising the data in a consistent manner for all seven data sets. However, it does not provide the correct value for p_c when the last data point is far away from p_c indicating that the energy release rate might not be the best quantity to analyze in order to obtain a predictive power. We will hence switch to the cumulative distribution in order to investigate this aspect as well as further test the critical point concept.

5 Analysis of the cumulative energy release

5.1 Power laws

Due to the noisy nature of data in general and especially the acoustic emission data analyzed here, a power law fit is not always numerically stable. The reason is the following: if the data exhibits rather large fluctuation in the end part, the search algorithm used in the optimization process of the fit will not necessarily find a local minimum for any choice of p_c larger than the last point p_{last}, driving the search towards a choice $p_c < p_{\text{last}}$ and thus creating a numerical instability. Of the 7 data sets considered here only 4 data sets, sets 1, 2, 5, 7 achieved (a single) numerically stable power law fit for the entire data interval (except the part below 100 bars that has been omitted as previously mentioned) as shown in Figure 2. Data sets 3 and 4 had to be truncated in the lower end at a point where a change of regime could be identified as a "kink" in the curve. Data set 6 could not be parameterised by a power law due to a kink in the last part of the data. In Table 2, the values for the physical parameters p_c and z are listed. We see that only for data sets 3 and 4 the power law does a good job of estimating p_c whereas it overshoots for data sets 1 and 2. For data sets 5 and 7 where the last point is far away from p_c, only in the first case do we get a reasonable estimate of p_c.

Table 2. Parameter values for fits with equation (1) to the cumulative energy released. The fits are shown in Figure 2.

Set #	fit p_c	z	t_{last}	true p_c
1	756	-1.7	713	713
2	718	-2.4	673	673
3	770	0.26	765	764
4	756	0.25	753	756
5	747	-1.6	713	797
7	666	-0.33	661	797

Figure 3 provides a non-parametric visual test of the critical point concept. We show the logarithm of the cumulative energy release as a function of the logarithm in base 10 of the distance $(p_c - p)/p_c$ to the critical rupture pressure p_c determined from the fits shown in Figure 2. While the power law regime qualified by a straight line in this representation does not extend to many decades, the plots shown in Figure 3 are nevertheless suggestive of a critical point. The relative range of pressure-to-failure $(p_c - p)/p_c$ defining the critical regime is limited by the resolution in pressure which is here no better than one bar and thus limits the investigation of the energy release rate closer to the rupture.

The over-all conclusion of the analysis presented here is that a pure power law does a reasonable job

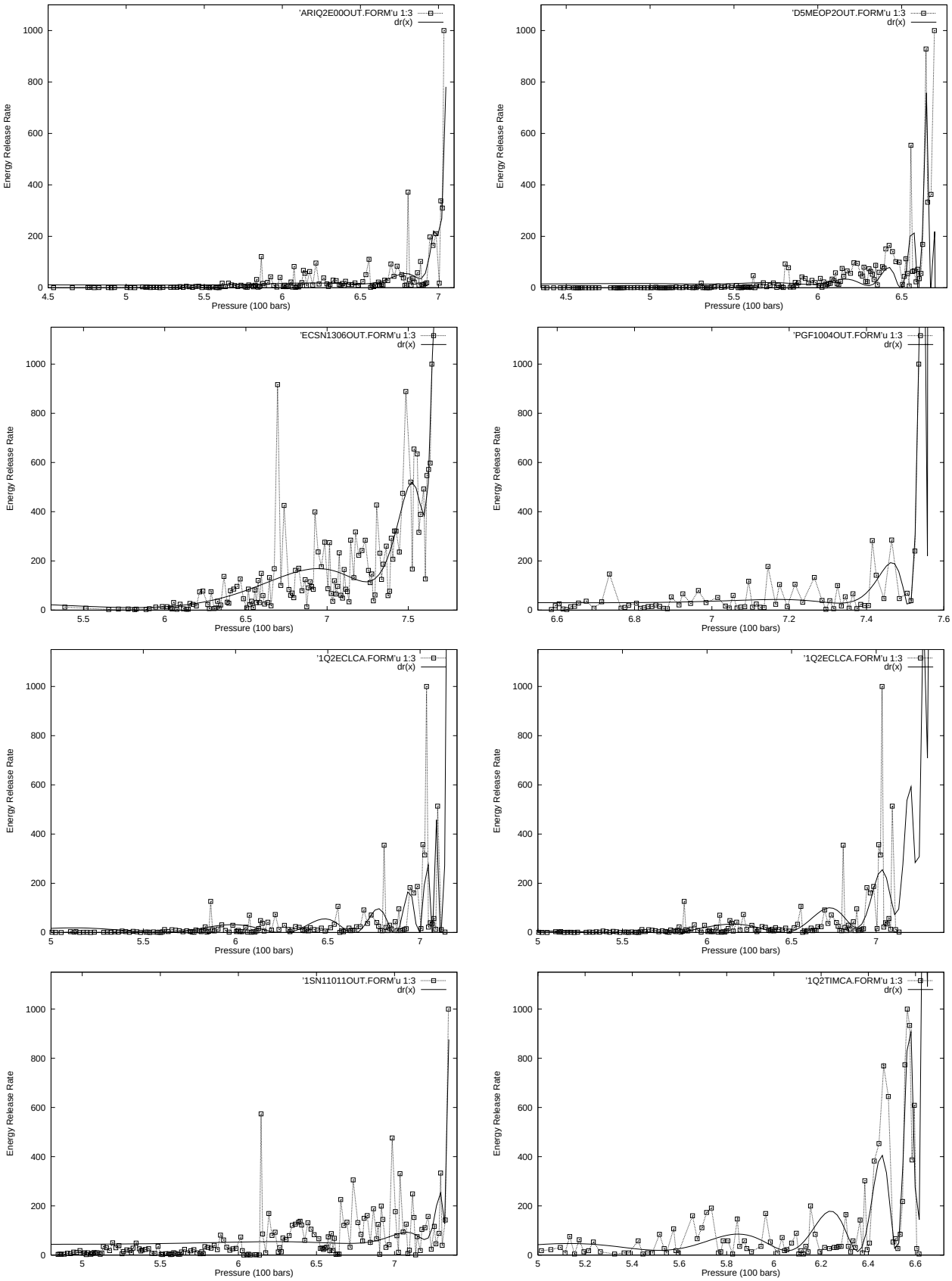

Fig. 1. Starting from the upper left corner and reading from left to right and from top to bottom as in a book, we show the best fit of the energy release rate with equation (2) for data set 1, 2, 3, 4, 5 (best and second best), 6 and 7. Notice how the log-periodic oscillations allow to account for an accelerating rate of bursts on the approach of the rupture.

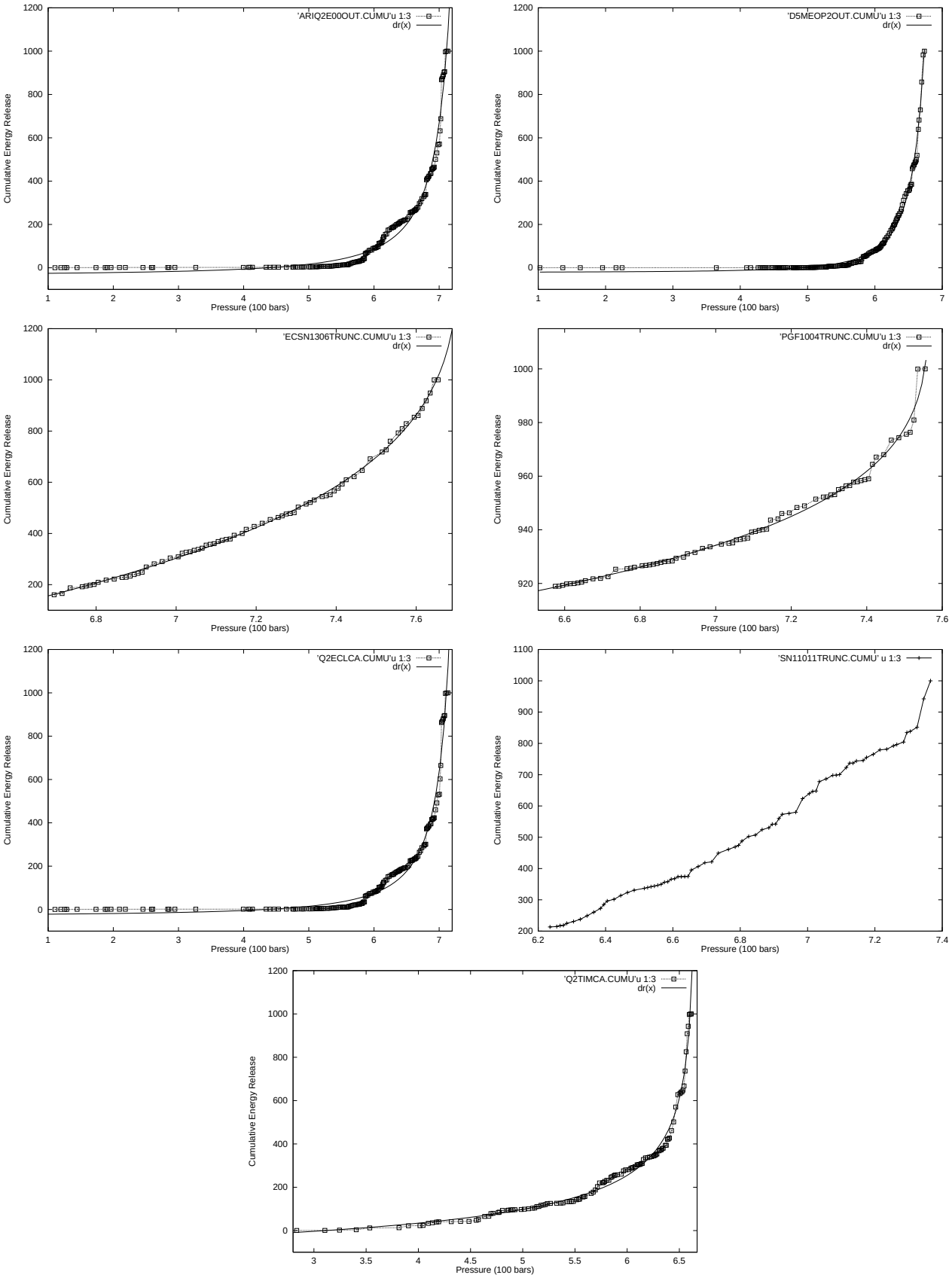

Fig. 2. Cumulative energy release fitted with equation (1). Starting from the upper left corner and reading from from left to right and from top to bottom as in a book, we have data set 1, 2, 3, ...7. Data sets 3 and 4 have been truncated in the lower end, taking as the first point the point where the acceleration in the acoustic emission begins in a similar way as for the other data sets. A unit of the abscissa corresponds to 100 bars.

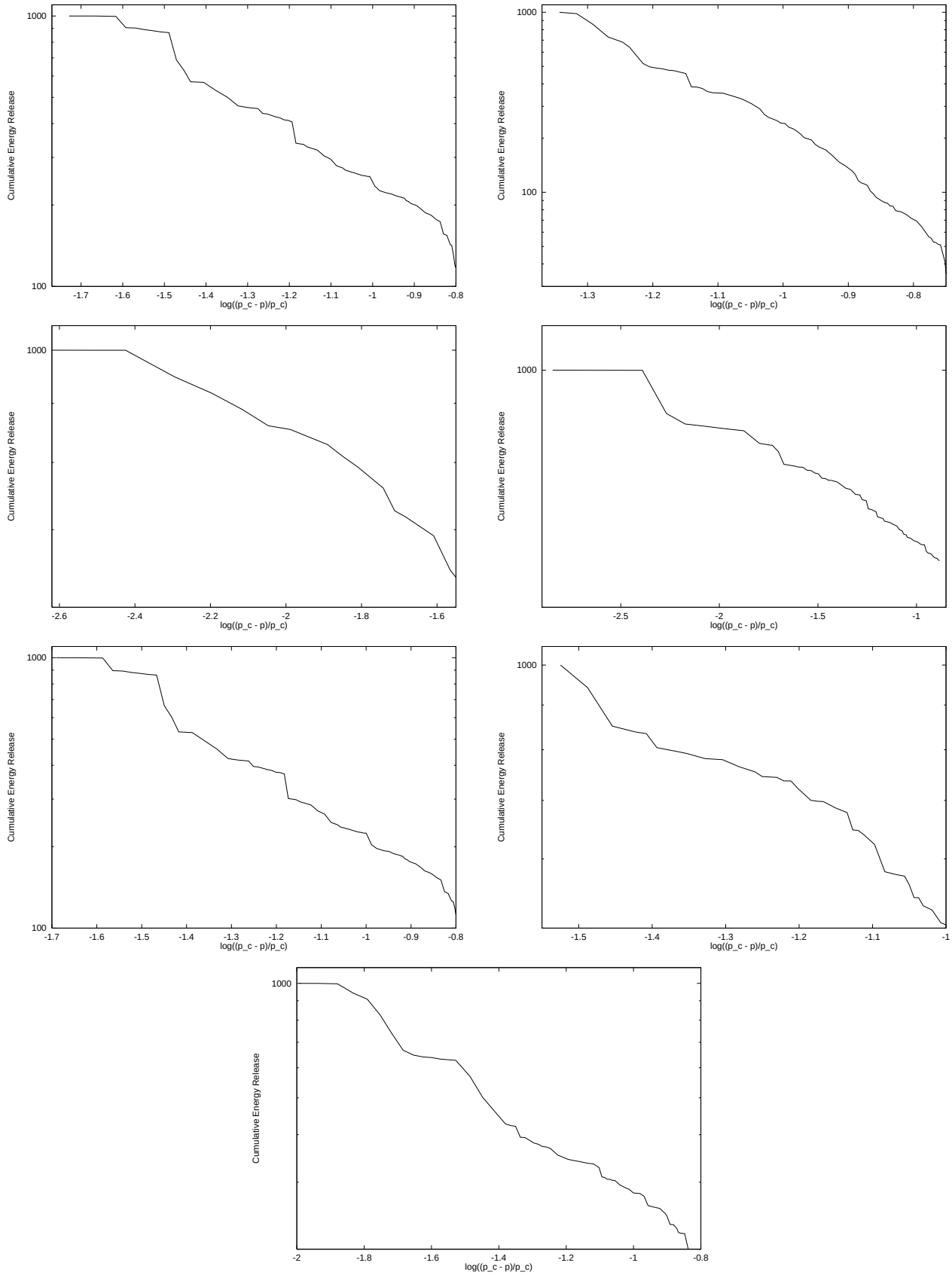

Fig. 3. Cumulative energy release (in $\ln_{10}$ scale) as a function of the logarithm (base 10) of the distance $(p_c - p)/p_c$ to the critical rupture pressure p_c determined from the fits shown in Figure 2. Starting from the upper left corner and reading from from left to right and from top to bottom as in a book, we have data set 1, 2, 3, ...7. We show the last "critical region" close to rupture which is suggestive of a power law qualified by a straight line in this representation.

of parameterising the cumulative data but does not seem to provide for a predictive tool: truncating the data in the upper end will only increase the over-shooting. We hence have to move beyond pure power laws in order to be able to use the cumulative energy release for prediction purposes. It is not very surprising that a pure power law fails to capture essential features of the data. Whether one believes in log-periodic oscillations or not, the analysis presented in the previous section clearly shows that the energy release rate is quite intermittent. The low-pass filtering performed in calculating the cumulative energy release have reduced these fluctuations to a large extent but clearly not enough. Secondly, it is clear that a truncation of the data in the lower end is necessary in order to identify the transition point to a power law acceleration. In fact, the identification of this transition point between random and cooperative behavior may very well be *the crux* when it comes to predictability.

We will thus investigate whether equations (2, 3) do a better job of parameterising the cumulative data. The rationale behind the last extension to equation (3) is that we cannot hope for a prediction capability if we cannot to a reasonable extent capture the features of the full data set which contains a transition in the acceleration of the energy release rate.

5.2 Beyond pure power laws

5.2.1 Fit with equation (2)

It is well-known that calculating the cumulative of some quantity effectively corresponds to performing a low-pass filtering thus diminishing fluctuations in the data. However, it will not completely remove them and thus a residue of the oscillations found in Section 4 should still be present in the data. Furthermore, adding an extra degree of freedom in the equation to be fitted will remove the problem with the numerical instability, since by the very nature of the experiments the fluctuation around some average behaviour will be slower for low pressures and more rapid for higher pressures. Equations (2, 3) exactly takes such a behaviour into account. This means that from a purely technical perspective, equations (2, 3) offers significant advantages to equation (1).

In Figure 4, we see the fits of 6 of the 7 data sets with equation (2). Whereas the fits with equation (1) in all cases only provided us with a single fit (or in the case of data set 6 none), we now have several solutions per time series. The fits shown in Figure 4 and the corresponding parameter values listed in Table 3 are those of the best fit which fulfills the criteria previously given. Data set 2 did not give any such fits, since $\omega \ll 1$ for all of them.

5.2.2 Fit with equation (3)

As previously mentioned, a transition point exists where the acceleration in the energy release rate increases significantly. Standard theoretical arguments from critical phenomena [45] suggest that the acceleration is approximately exponential before the transition point and goes to a power law after the transition point up to the critical point, hence defining the so-called critical region. As a justification of equation (3), we stress that such a cross-over has already been studied in detail in a numerical model of rupture [35]. We thus propose that equation (3) might provide a better fit of the data sets without the need of truncation as was the case in Section 4. By using equation (3), we are introducing an additional parameter, the typical width τ of the critical region, and a better fit is thus expected. However, if we also get a better estimate of p_c and a better predictive power, we can argue that this transition in the acceleration is indeed captured by equation (3).

Table 3. Parameter values for fits with equation (2) to the cumulative energy released. The fits are shown in Figure 4.

Set #	# fits	fit p_c	true p_c	t_{last}	z	ω
1	2	760	713	713	-1.7	13.0
3	2	774	764	765	0.13	6.0
4	3	757	756	755	0.23	5.0
5	3	734	797	713	-1.2	8.9
6	4	759	734	736	-0.98	2.4
7	2	669, 668	797	661	$-0.42, -0.43$	3.1, 8.6

Figures 5 and 6 show the fits of the seven data sets with equation (3). Sets 1–4 and 6 have one acceptable solution while two solutions are given for data sets 5 and 7. There are more solutions but most can be discarded or aggregated. The reason for the large number of minima for data sets 3, 4 and 7 is due to a degeneracy with respect to the new parameter τ, when the number of data points is small (72, 73 and 119 respectively). Thus, in these data sets, τ is not constrained well. If one insists that two solutions are identical if they have approximately the same values for ω and z, then the number of minima are reduced to approximately 15, 11 and 5. For data set 5, the best solution is shown together with the solution which had ω closest to 2π, a value that has been found repeatedly in previous works [25,27,28] and argued to be close to the universal mean field value [26]. For data set 7, the best solution is shown together with the only solution which did not have p_c close to p_{last}.

Comparing the results presented in Tables 3 and 4, a major improvement is obtained for data sets 1 and 2 by using equation (3) compared to equation (2). For data sets 3, 5 and 7, the improvement is minor while, for data sets 4 and 6, we get the same solutions. Hence, the overall conclusion is that equation (3) better captures important features in the data and supports the idea of a transition in the acceleration of the energy release rate from exponential to power law.

6 Prediction of the critical pressure of rupture

Armed with these empirical tests of the concept of critical rupture, prediction should in principle be possible by extrapolation of the acoustic emission data using the theoretical formulas. This scheme is similar to that proposed

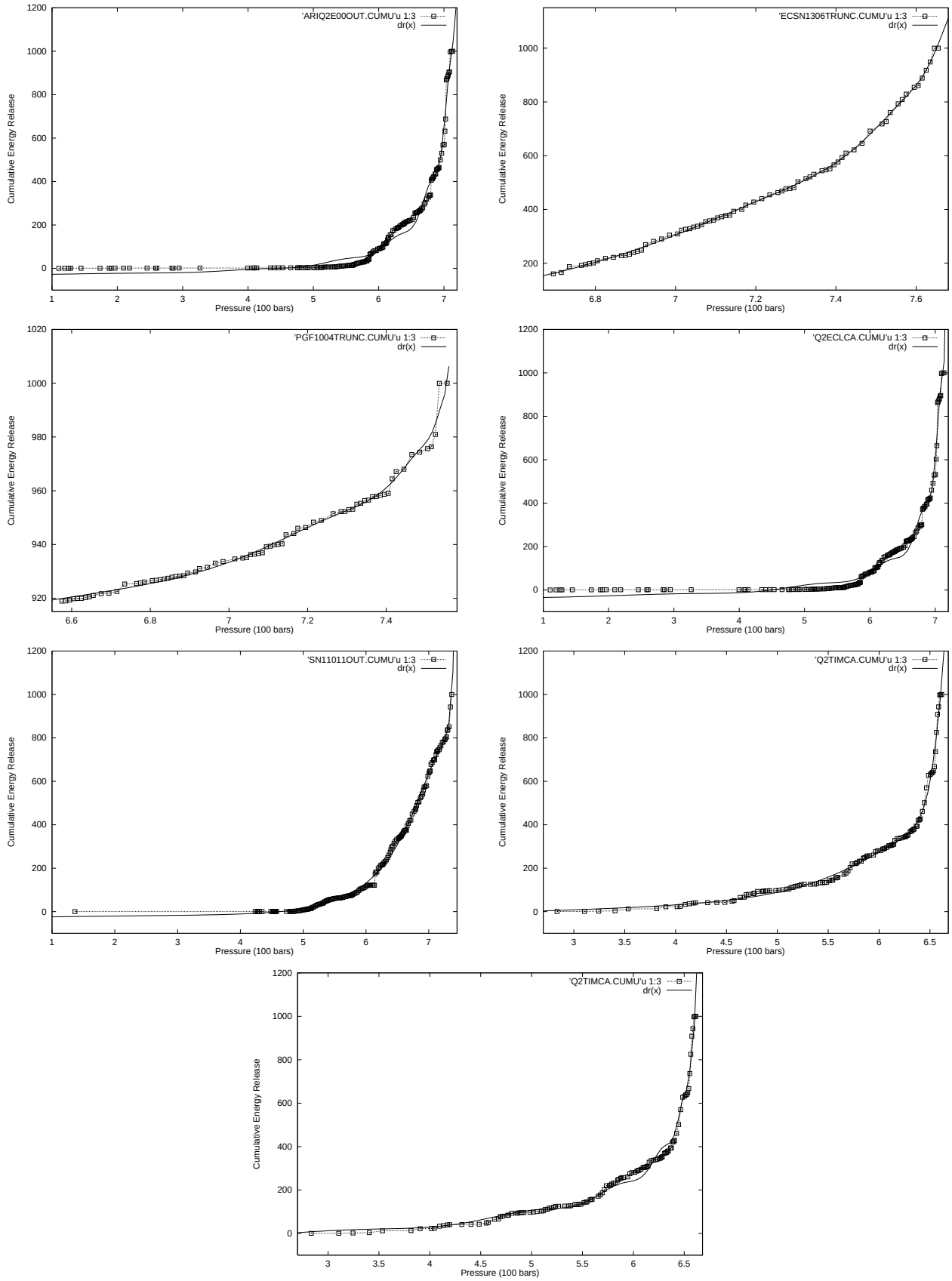

Fig. 4. Cumulative energy release fitted with equation (2). Starting from the upper left corner and reading from from left to right and from top to bottom as in a book, we have data set 1, 3, 4, 5, 6, 7 (first minimum) and 7 (second minimum). Data sets 3 and 4 have been truncated in the lower end, taking as the first point the point where the acceleration in the acoustic emission begins to be similar to the other data sets.

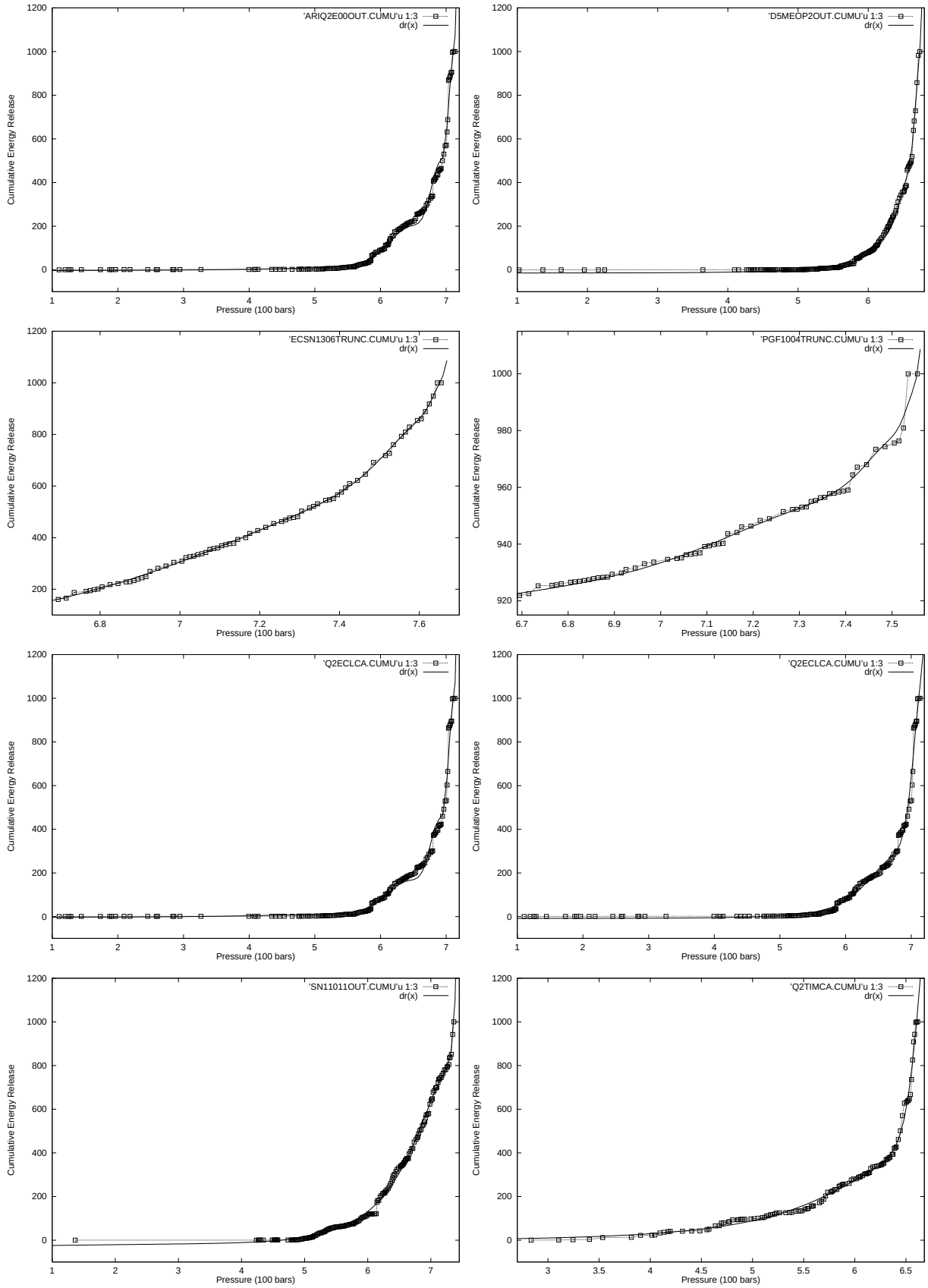

Fig. 5. Cumulative energy release fitted with equation (3). Starting from the upper left corner and reading from from left to right and from top to bottom as in a book, we have data set 1, 2, 3, 4, 5, 6, 7 (first minimum). Data sets 3 and 4 have been truncated in the lower end, taking as the first point the point where the acceleration in the acoustic emission begins to be similar to the other data sets.

Table 4. Parameter values for fits with equation (3) to the cumulative energy released. The fits are shown in Figures 5 and 6.

Set #	# fits	fit p_c	true p_c	t_{last}	z	ω	τ
1	3	727	713	713	-0.57	8.6	1.8
2	1	705	673	673	-1.7	13.4	1.4
3	33	767	764	765	0.52	4.5	1.0
4	15	757	756	755	0.23	5.0	428
5	4	728, 743	797	713	$-0.8, -1.1$	8.7, 6.7	1.9, 1.9
6	4	759	734	736	-0.98	2.4	124
7	17	668, 699	797	661	$-0.33, -1.3$	3.0, 4.4	2.3, 1.9

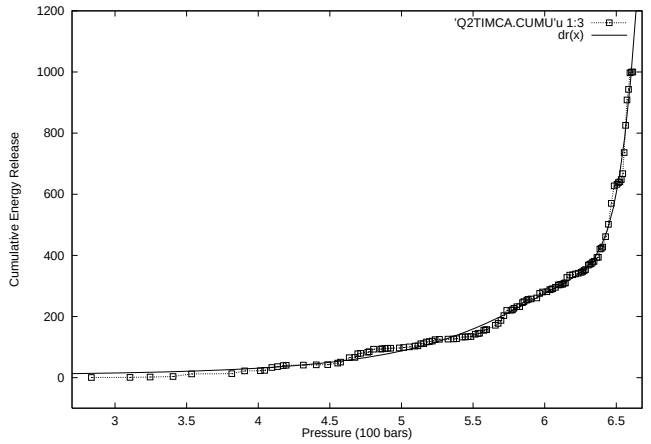

Fig. 6. Second solution of the cumulative energy release of data set 7 fitted with equation (3).

Table 5. Summary of the predicted critical pressures and comparison with the true pressure at rupture using equation (1) on the seven pressure tanks.

Set #	fit p_c	true p_c	t_{last}	z
1	749	713	705	-1.5
1	739	713	707	-1.3
1	739	713	709	-1.3
3	819	764	742	-0.02
3	750	764	746	0.67
3	753	764	751	0.60
3	755	764	753	0.58
3	758	764	756	0.50
3	764	764	759	0.39
3	769	764	761	0.29
3	770	764	763	0.27
4	809	756	744	-0.64
4	754	756	748	0.30
4	772	756	751	-0.05

by Voight to describe and predict rate-dependent material failure [46], based on the use of an empirical power law relation supposed to be followed by an observable variable. However, Voight's procedure is impractical due to the narrowness of the domain of validity of the pure power law, preventing a realistic implementation of the prediction. This will be confirmed by our tests presented below with equation (1). In order to extend the domain of validity beyond the rather narrow critical region, we are then going to test for the predictive merits of equations (2, 3).

The question we now address is whether we can use equations (1–3) in order to predict from the value of p_c the approximate value of the pressure at rupture. Data sets 5 and 7 being incomplete, *i.e.*, having acoustic emissions recorded up to a value p_{last} far from the pressure at rupture (11% below p_c for data set 5 and 17% below p_c for data set 7), this prediction question has already been answered to some extent. For data set 5, equation (1) gave just as good result as equation (3), the result with equation (2) being slightly worse. Choosing the second solution for equation (3), the estimate of p_c in these three cases was obtained with an error of 6%, 9% and 7%, respectively. For data set 7, equations (1) and (2) only gave solutions with $p_c \approx p_{last}$, the usual signature that the prediction is not reliable because it is controlled by the very last acceleration. In contrast, equation (3) produces a better solution with an error of 12% which can be compared with the difference of 17% between p_c and p_{last}.

Since the results for data set 7 using the entire data set are not very good (presumably because p_{last} is so far away from p_c), it does not seem reasonable to include this data set in a prediction scheme. Of the remaining data sets, the first prediction attempt for data set 1 was made for $p \approx 676$, for data set 2 it was 629, for data set 3 it was 742, for data set 4 it was 733, for data set 5 it was 687 and for data set 6 (which had no solutions for Eq. (1)) it was 688. These truncations were based on purely numerical consideration, *i.e.*, how many data points can one afford to remove without severely increasing the degeneracy of the cost-function used in the optimization of the fit. As a consequence, a maximum of 30 points were removed from the larger data sets (≈ 170 points for data sets 1,2,5 and 6) and 20 points from the smaller data sets (≈ 70 for data sets 3 and 4).

As we can see from Table 5, the prediction performance of equation (1) is quite bad and only data set 3 gives something interesting.

In Tables 6–11, we see the corresponding results using equation (2). Again the prediction performance is not good.

In Tables 12–17 we see the corresponding results using equation (3). When two solutions are given, the first is the best fit and the second is the best fit with ω closest to 2π. If two fits have ω's approximately at the same distance from 2π then both are listed. If only one fit is listed, then ω of this fit was also closest to 2π. We also demand that p_c is not very close to p_{last}. The reason for including these

Table 6. Same as Table 5 with equation (2) on the pressure tank 1.

Set #	# fits	fit p_c	true p_c	t_{last}	z	ω
1	1	947	713	684	−1.6	5.1
1	1	922	713	689	−0.75	3.1
1	1	939	713	698	−0.48	1.4
1	2	728	713	705	−0.96	7.8
1	1	756	713	707	−1.7	12.2
1	1	757	713	709	−1.7	12.4

Table 7. Same as Table 5 with equation (2) on the pressure tank 2.

Set #	# fits	fit p_c	true p_c	t_{last}	z	ω
2	1	658	673	651	−0.03	1.5
2	3	667	673	653	−0.43	1.8
2	1	656	673	655	−0.22	1.4
2	1	668	673	657	−2.1	2.6
2	1	668	673	657	−2.1	2.6
2	1	776	673	661	−2.5	3.3
2	2	795	673	664	−2.7	3.9

Table 8. Same as Table 5 with equation (2) on the pressure tank 3.

Set #	# fits	fit p_c	true p_c	t_{last}	z	ω
3	3	755	764	746	0.62	13.0
3	5	757	764	751	0.63	12.6
3	5	757	764	753	0.54	13.8
3	3	762	764	756	0.37	5.0
3	1	823	764	759	−0.77	10.6
3	1	797	764	761	−0.29	8.4
3	1	774	764	761	0.12	6.0

Table 9. Same as Table 5 with equation (2) on the pressure tank 4.

Set #	# fits	fit p_c	true p_c	t_{last}	z	ω
4	2	738, 748	756	737	0.85, 0.59	3.3, 4.8
4	1	775	756	739	0.20	8.1
4	1	752	756	741	0.57	5.1
4	4	756	756	744	0.40	6.1
4	2	780	756	748	−0.16	10.4
4	2	769	756	751	−0.09	8.5

Table 10. Same as Table 5 with equation (2) on the pressure tank 5.

Set #	# fits	fit p_c	true p_c	t_{last}	z	ω
5	1	815	797	694	0.31	11.1
5	3	709, 724	797	703	−0.71, −0.92	1.8, 7.3
5	2	745	797	705	−2.4	3.2
5	1	723	797	707	−0.85	7.3
5	2	721	797	709	−0.79	7.1

Table 11. Same as Table 5 with equation (2) on the pressure tank 6.

Set #	# fits	fit p_c	true p_c	t_{last}	z	ω
6	1	737	734	690	−1.9	2.9
6	1	744	734	692	−2.4	2.9
6	2	936	734	711	−2.4	4.5
6	2	925	734	716	−2.0	4.3
6	4	924	734	719	−2.7	4.6
6	1	810	734	723	−0.88	2.9
6	1	802	734	726	−0.92	2.8
6	1	792	734	729	−0.60	2.7

additional fits is to illustrate whether one always get a solution with a p_c close to the true p_c or not.

As mentioned, numerical degeneracy of the cost-function used in the optimization of the fit with equations (2, 3) can be a problem when the number of data points is not large. Hence, we have recorded the predicted p_c as a function of p_{last} for all fits with equations (2, 3) obeying the constraints on ω previously mentioned. The results are shown in Figures 7 and 8. Whereas no pattern can be identified using equation (2) we do see a clustering around the true t_c using equation (3) for all data sets except 6.

7 Conclusion

Considering the limited quality of the data recorded in a sub-optimal industrial environment, it is quite interesting that a reasonably clear picture has emerged from the analysis presented here. Beginning with the log-periodic analysis of the energy release rate, it is remarkable that the parameter values for the exponent z and log-periodic angular frequency ω obtained from the fits with equation (2) to the 7 first data set actually agree on $z \approx -1.4 \pm 0.7$ and $\omega \approx 5$ or $\omega \approx 10$ corresponding to a frequency doubling as seen in Table 2. Furthermore, from Figures 2 and 3, it is clear that at least 6 of the data sets exhibit an average power law acceleration as $p \to p_c$. The consistent results obtained for the energy release rate with respect to log-periodic oscillations is reasonably confirmed by the results obtained with equation (3), see Table 4 and Figures 5 and 6. Comparing these results with those obtained with equation (2) suggest that the cumulative energy release does exhibit a transition from an approximately exponential increase to that of a power law, in agreement with the numerical simulations of Sornette and Andersen [35]. Additional support for such a transition comes from the better predictions results obtained using equation (3) instead of equation (2).

The general results for the predictive power of equations (1–3) is that the first two equations do not perform at all. The results with equation (3) are more positive. For data set 1, we get a suggestion for $p_c \approx 720$ bars already at $p_{last} \approx 682$ bars while the true rupture occurred at 713 bars. For data set 2, we start to get a reasonable stable estimate $p_c \approx 680 - 90$ bars for $p_{last} \approx 651$ bars with some prior indications down to $p_{last} \approx 621$ bars, while the true rupture occurs at 673 bars. For data set 3, the results are

Table 12. Same as Table 5 with equation (3) on the pressure tank 1.

Set #	# fits	fit p_c	true p_c	t_{last}	z	ω	τ
1	1	850	713	678	−2.4	5.6	530
1	2	761, 831	713	680	−1.4, −1.7	11.4, 5.6	1.7, 5.8
1	1	723	713	682	−0.45	6.9	1.7
1	5	732, 714	713	684	−0.07, −0.09	9.4, 6.8	1.4, 1.5
1	2	733, 728	713	687	0.14, 0.15	10.3, 9.3	1.4, 1.4
1	3	702, 1070	713	689	0.19, −2.4	5.1, 5.4	1.6, 24
1	4	738, 1093	713	691	0.10, −2.2	11.1, 5.1	1.4, 32
1	3	859, 730	713	698	0.75, −1.6	1.0, 2.8	6.8, 10
1	3	763	713	701	−2.4	4.3	10.0
1	1	711	713	703	−2.4	5.7	1.8
1	9	711, 713	713	705	−0.14, −0.17	5.3, 5.8	2.0, 1.7
1	5	712	713	707	−0.17	5.5	2.0
1	6	715	713	709	−0.24	6.2	1.9

Table 13. Same as Table 5 with equation (3) on the pressure tank 2.

Set #	# fits	fit p_c	true p_c	t_{last}	z	ω	τ
2	1	690	673	629	−2.6	2.6	6.8
2	3	726, 682	673	631	0.51, −1.5	1.3, 2.5	2.4, 8.9
2	1	693	673	633	−1.1	2.5	6.2
2	4	752, 672	673	635	0.49, −2.5	1.3, 3.2	2.4, 7.5
2	3	735, 762	673	638	0.26, −2.9	2.7, 3.5	2.3, 44
2	2	756	673	640	−2.4	3.3	16.0
2	2	866, 683	673	644	−1.7, −2.8	2.2, 3.4	3.1, 9.5
2	1	722	673	648	−1.7	2.7	13
2	4	657, 696	673	651	0.08, −2.1	1.5, 2.5	18, 13
2	4	657, 689	673	653	0.50, −1.6	1.5, 2.5	2.8, 9.0
2	4	659, 747	673	655	−0.43, −2.7	1.8, 3.9	3.5, 5.2
2	2	678, 766	673	657	−2.1, −2.2	2.6, 3.1	887, 63
2	3	685	673	659	−1.8	3.2	3.5
2	9	695, 697	673	664	−2.6, 2.8	3.0, 3.1	67, 69

Table 14. Same as Table 5 with equation (3) on the pressure tank 3.

Set #	# fits	fit p_c	true p_c	t_{last}	z	ω	τ
3	8	898, 825	764	741	−2.7, −2.1	13.3, 6.8	227, 7.2
3	13	877, 803	764	744	−2.1, −1.0	13.4, 6.4	572, 8.1
3	8	752, 807	764	748	0.62, −1.2	12.0, 6.6	120, 4.7
3	8	758, 770	764	752	0.63, 0.44	4.0, 6.2	1.0, 1.3
3	2	760, 782	764	755	0.41, 0.09	4.9, 6.7	4.7, 1.8
3	2	863, 784	764	757	−1.60.12	13.2, 6.3	951
3	8	796, 784	764	760	−0.03, −0.04	9.0, 6.9	1.6, 6.5
3	2	772, 776	764	762	0.26, 0.09	5.6, 6.1	1.7, 27

Table 15. Same as Table 5 with equation (3) on the pressure tank 4.

Set #	# fits	fit p_c	true p_c	t_{last}	z	ω	τ
4	13	736, 752	756	733	0.86, 0.42	3.1, 5.9	2.4, 474
4	11	739, 758	756	735	0.78, 0.32	3.5, 6.7	52, 165
4	12	751, 760	756	737	0.63, 0.34	5.6, 6.7	1.8, 87
4	22	781, 767	756	739	0.16, 0.36	9.5, 7.0	3.3, 4.5
4	32	763, 759	756	741	0.79, 0.40	8.6, 6.2	1.1, 373
4	12	756, 759	756	744	0.40, 0.35	6.1, 6.4	428, 354
4	10	780, 758	756	748	−0.16, 0.30	10.3, 6.3	924, 16
4	10	769, 758	756	751	0.09, 0.30	10.3, 6.3	924, 16

Table 16. Same as Table 5 with equation (3) on the pressure tank 5.

Set #	# fits	fit p_c	true p_c	t_{last}	z	ω	τ
5	3	751, 717	797	687	−1.3, 0.06	13.6, 7.5	1.4, 1.5
5	3	739, 798	797	689	−0.08, −2.9	11.2, 8.6	1.4, 148
5	4	732, 762	797	691	−0.03, −2.5	9.8, 5.2	1.4, 11
5	3	705, 773	797	694	0.09, −2.4	5.6, 7.2	1.6, 2.9
5	1	765	797	698	−2.0	6.5	2.8
5	2	752, 758	797	701	−0.61, −2.1	11.1, 4.7	1.5, 4.6
5	10	710, 718	797	703	−1.8, −0.57	5.5, 6.2	2.0, 2.3
5	7	710, 722	797	705	−0.22, −0.85	5.1, 7.0	2.1, 12
5	7	712, 713	797	707	−0.28, 0.31	5.5, 5.9	2.1, 1.9
5	9	715	797	709	−0.38	6.2	2.0

Table 17. Same as Table 5 with equation (3) on the pressure tank 6.

Set #	# fits	fit p_c	true p_c	t_{last}	z	ω	τ
6	4	722, 745	734	688	1.3, −1.5	13.7, 5.3	1.1, 1.5
6	2	741, 867	734	690	−2.3, −2.8	2.8, 5.0	35, 897
6	7	763, 762	734	692	−1.4, −2.0	6.9, 6.1	1.6, 1.6
6	4	776	734	696	−2.0	6.7	1.9
6	4	724, 761	734	700	0.94, −2.2	12.2, 3.4	1.2
6	2	770	734	702	−2.8	3.3	7.5
6	7	729, 782	734	705	0.81, −2.4	12.4, 4.9	1.2, 3.0
6	2	722, 790	734	708	0.76, −2.0	10.6, 5.4	1.3, 3.5
6	6	746, 978	734	711	0.66, −2.6	11.1, 6.4	1.3, 6.1
6	7	753, 820	734	713	0.67, −2.7	12.8, 5.2	1.3, 5.6
6	6	730, 812	734	716	0.86, −2.3	12.9, 4.7	1.2, 5.5
6	8	839, 914	734	719	2.2, −2.0	3.3, 5.0	2.6, 6.2
6	7	921	734	723	−1.8	6.0	4.5
6	20	759, 892	734	726	1.0, −2.7	2.0, 4.4	2.9, 5.6
6	13	883	734	729	−1.8	4.9	4.0
6	13	785, 889	734	732	1.6, −0.03	2.4, 6.1	2.5, 3.0

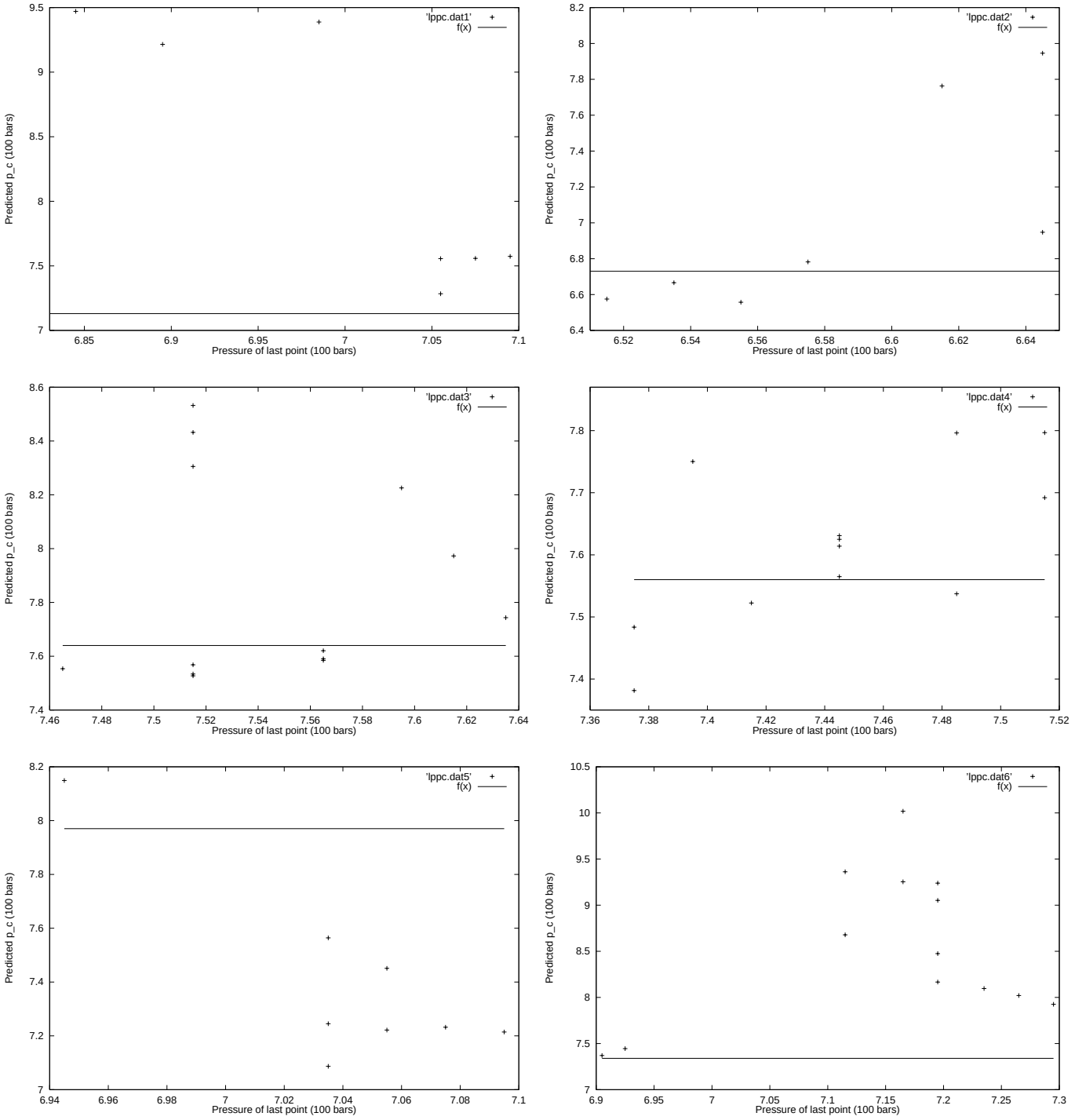

Fig. 7. Compilation of all predicted p_c as a function of p_{last} using equation (2). The straight line represent the true p_c.

not very convincing, as we get good solutions only close to the true p_c. It is interesting to note that if we *only* consider solutions with $\omega \approx 2\pi$, then we get a good estimate for $p_{last} \approx 752$ bars while the true rupture occurs at 756 bars. Remarkably, the same is true for data set 4 all the way down to the lowest pressure of ≈ 733 bars used, while the true rupture occurs at 756 bars. Data set 5 is as mentioned incomplete, the last point being ≈ 85 bars away from p_c. For this data set, we get a reasonable estimate on p_c if we focus on solutions with $\omega \approx 2\pi$ for p_{last} in the range of $689 - 701$, while the true rupture occurs at 791 bars. For higher pressures, the fits lock on p_c close to the last point in the untruncated data set. The results for data set 7 are very mixed without any clear pattern.

As seen in Figure 8, using all fits shows that a predictive potential of equation (3) exists since a clustering

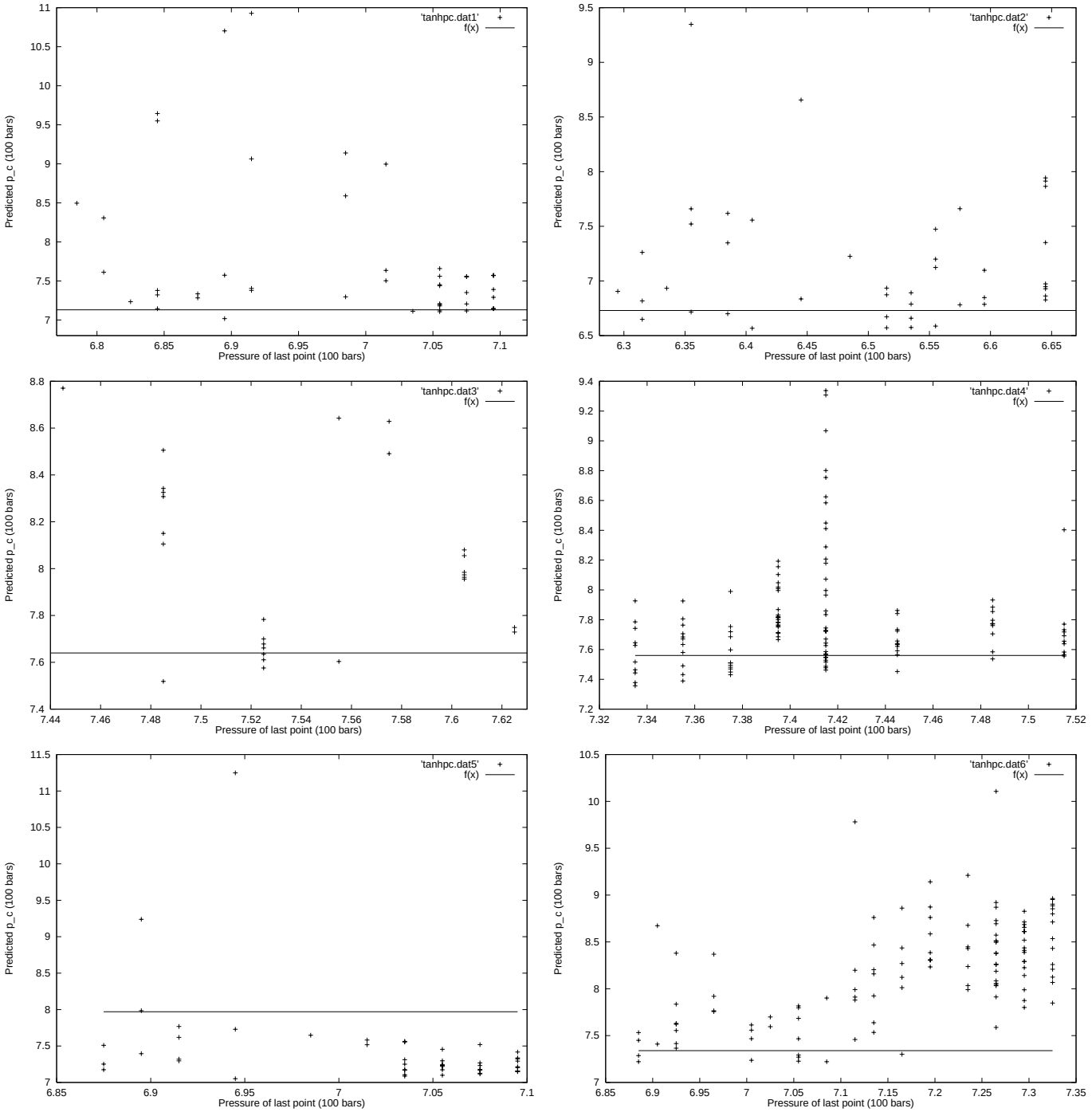

Fig. 8. Compilation of all predicted p_c as a function of p_{last} using equation (3). The straight line represent the true p_c.

of the predicted p_c's occurs around the true p_c for all data sets except one (data set 7). This suggests that for a better controlled experimental situation, a reliable prediction procedure based on equation (3) can be achieved.

We thank J.-C. Anifrani from Aérospatiale-Matra Inc., Bordeaux, France, for sharing the data with us. This research was supported in part by NSF under the grant NSF-DMR99-71475.

References

1. T. Reichhardt, Nature (London) **384**, 99 (1996).
2. *"Fracture"*, edited by H. Liebowitz (Academic, New York, 1984), Vols. I-VII.
3. J. Fineberg, S.P. Gross, M. Marder, H.L. Swinney, Phys. Rev. Lett. **67**, 457 (1991); Phys. Rev. B **45**, 5146 (1992); S.P. Gross, J. Fineberg, M. Marder, W.D. McCormick, H.L. Swinney, Phys. Rev. Lett. **71**, 3162 (1993); F. Abraham, D. Brodbeck, R.A. Rafey, W.E. Rudge, Phys.

Rev. Lett. **73**, 272 (1994); B.L. Holian, R. Ravelo, Phys. Rev. B **51**, 11275 (1995); E.S.C. Ching, J.S. Langer, H. Nakanishi, Phys. Rev. E **53**, 2864 (1996); M. Marder, J. Fineberg, Physics Today **49**, 24 (1996); E. Sharon, J. Fineberg, Phys. Rev. B **54**, 7128 (1996).

4. B.B. Mandelbrot, D.E. Passoja, A.J. Paullay, Nature (London) **308**, 721 (1984); E. Bouchaud, G. Lapasset, J. Planes, Europhys. Lett. **13**, 73 (1990); K.J. Maloy, A. Hansen, E.L. Hinrichsen, S. Roux, Phys. Rev. Lett. **68**, 213 (1992); J. Schmittbuhl, S. Gentier, S. Roux, Geophys. Res. Lett. **20**, 639 (1993); J. Schmittbuhl, S. Roux, Y. Berthaud, Europhys. Lett. **28**, 585 (1994); T. Engoy, K.J. Maloy, A. Hansen. S. Roux, Phys. Rev. Lett. **73**, 834 (1994); P. Daguier, S. Henaux, E. Bouchaud, F. Creuzet, Phys. Rev. E **53**, 5637 (1996).
5. J.J. Gilman, Science **274**, 65 (1996); *Shear-induced chemical reactivity, in volume honoring the 90th birthday of Sir Nevill Mott, Metal-Insulator transitions revisited*, edited by P.P. Edwards, C.N.R. Rao (Taylor and Francis Ldt., London, 1995), p. 269.
6. A.R.C. Westwood, J.S. Ahearn, J.J. Mills, Colloids and Surfaces **2**, 1 (1981).
7. see for instance *Aging of US Air Force Aircraft, Final Report from the Committee on Aging of US Air Force Aircraft, National Materials Advisory Board Commission on Engineering and Technical Systems, National Research Council, Publication NMAB-488-2* (National Academy Press, Washington, D.C., 1997).
8. M. Ausloos, Solid State Commun. **59**, 401 (1986).
9. D. Stauffer, A. Aharony, *Percolation theory* (Taylor and Francis, London, 1992).
10. L. de Arcangelis, S. Redner, H.J. Herrmann, J. Phys. Lett. **46**, L585 (1985).
11. L. de Arcangelis, A. Hansen, H.J. Herrmann, S. Roux, Phys. Rev. B **40**, 877 (1989).
12. P.M. Duxbury, P.D. Beale, P.L. Leath, Phys. Rev. Lett. **57**, 1052 (1986); A. Gilabert, C. Vanneste, D. Sornette, E. Guyon, J. Phys. **48**, 763 (1987).
13. S. Roux, A. Hansen, H. Herrmann, E. Guyon, J. Stat. Phys. **52**, 237 (1988).
14. *Statistical models for the fracture of disordered media*, edited by H.J. Herrmann, S. Roux (Elsevier, Amsterdam, 1990); P. Meakin, Science **252**, 5003 (1991).
15. A. Hansen, E. Hinrichsen, S. Roux, Phys. Rev. B **43**, 665 (1991).
16. D. Sornette, T. Magnin, Y. Bréchet, Europhys. Lett. **20**, 433 (1992); Y. Bréchet, T. Magnin, D. Sornette, Acta Metallurgica **40**, 2281 (1992).
17. M. Mezard, G. Parisi, M.A. Virasoro, *Spin glass theory and beyond* (World Scientific, Singapore; New Jersey 1987).
18. D. Sornette, C. Vanneste, Phys. Rev. Lett. **68**, 612 (1992); C. Vanneste, D. Sornette, J. Phys. I France **2**, 1621 (1992); D. Sornette, C. Vanneste, L. Knopoff, Phys. Rev. A **45**, 8351 (1992).
19. D. Sornette, C. Vanneste, Phys. Rev. E **50**, 4327 (1994).
20. L. Lamaignère, F. Carmona, D. Sornette, Phys. Rev. Lett. **77**, 2738 (1996); Physica A **241**, 328 (1997).
21. R.M. Bradley, K. Wu, J. Phys. A **27**, 327 (1994); Phys. Rev. E **50**, R631 (1994).
22. J.-C. Anifrani, C. Le Floc'h, D. Sornette, B. Souillard, J. Phys. I France **5**, 631 (1995).
23. J.-C. Anifrani, C. Le Floc'h, D. Sornette, Contrôle Industriel **220**, 43 (1999).
24. H. Saleur, D. Sornette, J. Phys. I France **6**, 327-355 (1996).
25. Y. Huang, G. Ouillon, H. Saleur, D. Sornette, Phys. Rev. E **55**, 6433 (1997).
26. D. Sornette, Physics Reports **297**, 239 (1998).
27. D. Sornette, C.G. Sammis, J. Phys. I France **5**, 607 (1995); D. Sornette, A. Johansen, J.-P. Bouchaud, J. Phys. I France **6**, 167 (1996); G. Ouillon, D. Sornette, A. Genter, C. Castaing, J. Phys. I France **6**, 1127 (1996); A. Johansen, D. Sornette, H. Wakita, U. Tsunogai, W.I. Newman, H. Saleur, J. Phys. I France **6**, 1391 (1996); A. Johansen, H. Saleur, D. Sornette, Eur. Phys. J. B **15**, 551 (2000); H. Saleur, C.G. Sammis, D. Sornette, J. Geophys. Res. **101**, 17661 (1996); Y. Huang, H. Saleur, C.G. Sammis, D. Sornette, Europhys. Lett. **41**, 43 (1998).
28. D. Sornette, A. Johansen, A. Arneodo, J.-F Muzy, H. Saleur, Phys. Rev. Lett. **76**, 251 (1996).
29. K. Mogi, Bull. Eq. Res. Inst. Tokyo Univ. **47**, 395 (1969).
30. K. Mogi, J. Phys. Earth **43**, 533 (1995).
31. J.V. Andersen, D. Sornette, K.-T. Leung, Phys. Rev. Lett. **78**, 2140 (1997).
32. A. Aharony, Lecture Notes in Physics **186**, 209 (1983).
33. H.E. Daniels, Proc. Roy. Soc. London A **183**, 405 (1945); M.W. Suh, B.B. Battacharyya, A. Grandage, J. Appl. Prob. **7**, 712 (1970); P.K. Sen, J. Appl. Prob. **10**, 586 (1973); Ann. Stat. **1**, 526 (1973); D. Sornette, J. Phys. A **22**, L243 (1989).
34. S.J. Zhou, R. Blumenfeld, W.A. Curtin, B.L. Holian, Mat. Res. Soc. Symp. Proc. **409**, 267 (1996).
35. D. Sornette, J.V. Andersen, Eur. Phys. J. B **1**, 353 (1998).
36. M. Sahimi, S. Arbabi, Phys. Rev. Lett. **77**, 3689 (1996).
37. A. Johansen, D. Sornette, Int. J. Mod. Phys. C **9**, 433 (1998).
38. A. Garcimartin, A. Guarino, L. Bellon, S. Ciliberto, Phys. Rev. Lett. **79**, 3202 (1997); A. Guarino, A. Garcimartin, S. Ciliberto, Eur. Phys. J. B **6**, 13 (1998); A. Guarino, S. Ciliberto, A. Garcimartin, Europhys. Lett. **47**, 456 (1999).
39. A. Gilabert, A. Sornette, M. Benayad, D. Sornette, C. Vanneste, J. Phys. France **51**, 237 (1990).
40. A.A. Pollock, *Acoustic emission inspection, Metal Handbook*, Ninth edn, Vol. 17, Non-destructive Evaluation and Quality Control (ASM International, 1989), p. 278-294.
41. *First International Symposium on Acoustic Emission from Reinforced Composites, San Francisco, California, July 19-21, 1983* (The Society of the Plastic Industry).
42. Y. Huang, A. Johansen, M.W. Lee, H. Saleur, D. Sornette, *Artifactual Log-Periodicity in Finite-Size Data: Relevance for Earthquake Aftershocks*, in press in J. Geophys. Res. (preprint at `http://xxx.lanl.gov/abs/cond-mat/9911421`).
43. W.H. Press, B.P. Flannery, S.A. Teukolsky, W.T. Vetterling, *Numerical Recipes* (Cambridge University Press, Cambridge UK, 1992).
44. A. Johansen, D. Sornette, A.E. Hansen, Physica D **138**, 302 (2000).
45. N. Goldenfeld, *Lectures on Phase Transitions and the Renormalization Group* (Addison-Wesley, Advanced Book Program, Reading, Mass., 1992).
46. B. Voight, Science **243**, 200 (1989); Nature **332**, 125 (1988); B. Voight, R.R. Cornelius, Nature **350**, 695 (1991).